Journal of Alloys and Compounds 797 (2019) 1327–1337

Contents lists available at ScienceDirect

Journal of Alloys and Compounds

journal homepage: http://www.elsevier.com/locate/jalcom

Co effects on Cu-Ni-Si alloys microstructure and physical properties

Zhuan Zhao [a, b, c], Yi Zhang [a, b, c, *], Baohong Tian [a, b, c, **], Yanlin Jia [d, ***], Yong Liu [a, b, c], Kexing Song [a, b, c], Alex A. Volinsky [e]

[a] School of Materials Science and Engineering, Henan University of Science and Technology, Luoyang, 471023, PR China
[b] Collaborative Innovation Center of Nonferrous Metals, Henan Province, Luoyang, 471023, PR China
[c] Henan Key Laboratory of Nonferrous Materials Science and Processing Technology, Luoyang, 471023, PR China
[d] College of Materials Science and Engineering, Beijing University of Technology, Beijing, 100124, PR China
[e] Department of Mechanical Engineering, University of South Florida, Tampa, 33620, USA

ARTICLE INFO

Article history:
Received 17 March 2019
Received in revised form
7 May 2019
Accepted 12 May 2019
Available online 15 May 2019

Keywords:
Cu-Ni-Co-Si alloy
Precipitates
Microstructure
Crystal orientation relationship

ABSTRACT

The effects of Co on the Cu-Ni-Co-Si alloys' microstructure and mechanical properties were investigated. The Cu-1.5Ni-1.0Co-0.6Si and Cu-1.5Ni-1.5Co-0.6Si alloys with combined aging and 40–80% cold rolling were also investigated. The hardness, electrical conductivity, and microstructure were characterized, complemented by X-ray diffraction analysis and transmission electron microscopy. At 450 °C alloys aging, the aging precipitated phases are β-Ni_3Si and Co_2Si. Specifically, the orthorhombic $(Ni, Co)_2Si$ precipitates were found, which have the same crystal structure as the Ni_2Si precipitates. The crystal orientation relationship between the matrix and the precipitates is: [112]Cu//[112]β//[012]p, $(1\bar{1}1)$Cu//$(1\bar{1}1)$β//(021)p; [001]Cu//[001]β//[001]p, (220)Cu//(110)β//(100)p. With the increasing Co content, the properties of the alloy were degraded. However, Co can promote the growth of the precipitates and accelerate precipitation during the aging process. After aging at 500 °C for 2 h, the hardness and conductivity of the Cu-1.5Ni-1.0Co-0.6Si alloy with 40% deformation were 250 HV and 43% IACS, respectively.

1. Introduction

Copper alloys are used for the lead frame, resistance welding electrodes, first wall of the nuclear reactor and so on [1–4]. Two types of ideal high-performance copper alloys are required for large scale integrated circuits. One is the high strength and high conductivity, requiring the tensile strength to be ≥ 600 MPa and conductivity ≥80% IACS, and the other is high strength and medium conductivity, requiring the tensile strength of ≥800 MPa and conductivity ≥50% IACS [5–8]. The Cu-Ni-Si alloy is the second type alloy, as mentioned above. It is being considered for applications in large-scale integrated circuits.

The phase transformations and related size, type and distribution of precipitated phases are the key factors to obtain the ideal Cu alloy with high strength and high conductivity [9–14]. Multiple research reports have indicated that the addition of trace elements, such as Mg [15,16], Cr [17,18], Zr [19,20], and Ag [21] can effectively improve the conductivity and strength of the Cu-Ni-Si alloys. Co is a very important element widely used in semiconductor electronic devices. Krishna et al. found that the increase in hardness and conductivity during aging was mainly attributed to the formation of fine Ni_2Si and Co_2Si precipitates in the Cu-Ni-Si-Co alloy [22]. Huang et al. found that a small amount of Co replaced Ni, forming $(Ni, Co)_2Si$ precipitates in the Cu-Ni-Si-Co alloy, which has better strength, hardness, and conductivity [23]. Ozawa et al. reported that the 0.6% Co and 1.0% Co alloys at 525 °C and 425 °C produced orthorhombic $(Ni, Co)_2Si$ precipitates that have the same crystal structure as the Ni_2Si precipitates formed in the alloy without Co [24]. Based on the previous study, it was found that a certain amount of Co atoms in the Cu-Ni-Si alloy will replace Ni to form $(Ni, Co)_2Si$. From the atomic ratio, in order to completely form $(Ni, Co)_2Si$ precipitates during aging, the addition of 1.0 wt% Co in the Cu-1.5Ni-0.6Si alloy was considered. In addition, in order to compare the effects of Co addition on the structure and performance of the Cu-1.5Ni-0.6Si alloy, the 1.5 wt% Co was also used in this experiment.

* Corresponding author. School of Materials Science and Engineering, Henan University of Science and Technology, Luoyang, 471023, PR China.
** Corresponding author. School of Materials Science and Engineering, Henan University of Science and Technology, Luoyang, 471023, PR China.
*** Corresponding author.
E-mail addresses: zhshgu436@163.com (Y. Zhang), bhtian007@163.com (B. Tian), jiayanlin@126.com (Y. Jia).

https://doi.org/10.1016/j.jallcom.2019.05.135
0925-8388/

The Cu-1.5Ni-1.0Co-0.6Si and Cu-1.5Ni-1.5Co-0.6Si alloys were aged at 350–550 °C with 40–80% cold deformation, providing an effective way to improve the Cu-Ni-Si alloy performance. The solid solution and aging strengthening mechanisms, including dislocation strengthening, precipitated phase strengthening, and the kinetic transformations of the Cu-1.5Ni-1.0Co-0.6Si and Cu-1.5Ni-1.5Co-0.6Si alloys were investigated in this paper. The optimized experimental processes included cold deformation after solidification and aging after cold deformation, followed by additional aging. The microstructure evolution of the two alloys was observed by optical and transmission electron microscopy during the aging process, and the twin crystals, precipitated phases and dislocations were also observed. The relationships between the conductivity and hardness during the aging of the alloy were analyzed. The twinning mechanism of the alloy and its effects on physical properties were analyzed. The aging strengthening mechanism and the aging precipitation kinetics of the alloy were also analyzed. Specifically, the effects of Co addition on the microstructure of the alloy were studied.

2. Experiment

The composition of the experimental Cu-Ni-Si alloys is listed in Table 1. The 99.95 wt% standard cathode copper Cu-CATH-2, Ni with 99.95% purity, Si with 99.95% purity and Cu-15 wt% Co master alloy were prepared and then melted in the vacuum induction furnace under an argon atmosphere, which prevented the alloy from oxidation. After heating the ingot in the furnace at 1000 °C for 1 h to reduce the number of surface defects, the XJ-500 metal profile extruder was used to make bars with Φ35 mm diameter. The samples were solution treated at 900 °C for 2 h by using the KSS-1200 tubular resistance furnace and water quenched. The cylinders were machined into the sheets with a size of 100 mm × 5 mm × 1 mm. Then, the samples with the surface oxide removed by acid pickling were deformed to 40% and 80% deformation with the C33150 rolling machine. The aging temperature was 350 °C, 400 °C, 450 °C, 500 °C, and 550 °C, and the aging time was 0.25 h, 0.5 h, 1 h, 2 h, 4 h, 6 h, 9 h, and 12 h, respectively.

The ZY9987 digital multimeter was used to measure the electrical resistance with ≤0.02 mΩ measurement error, and each sample was measured five times to obtain the average resistance value. Then, the sample thickness and width were also measured to calculate the conductivity following the YS/Z 478–2005 standard.

The hardness was measured using the HVS-1000 hardness tester. The sample size was 10 mm (length) × 5 mm (width) × 1 mm (thickness), according to the GB/T4340.1–1999 standard. The samples were polished before hardness measurements. Vickers hardness was measured at least 10 times to obtain the average value. The load was 100 g held for 15 s with 5% measurement error. After rough grinding, fine grinding, mechanical polishing, and etching, the microstructure was observed by the OLYMPUS PMG3 optical microscope. Ferric chloride (5 g) + hydrochloric acid (20 ml) + deionized water (100 ml) solution was used for etching. Transmission electron microscopy (TEM) and high-resolution TEM (HRTEM) images were obtained using the JEM-2100F transmission electron microscope with an operating voltage of 200 kV and 0.19 nm resolution.

3. Results

3.1. Optical microstructure

Fig. 1 shows optical images of the as-cast and solid-solution microstructure of the Cu-1.5Ni-1.0Co-0.6Si and Cu-1.5Ni-1.5Co-0.6Si alloys. The typical dendritic structure was observed in the as-cast samples, which is due to the rapid cooling rate caused by the uneven composition. There's a large temperature gradient at the early stage of solidification, thus the dendrite grows rapidly, and the sides of the dendrite axis form large branches. According to the measurements, the dendrite spacing of the Cu-1.5Ni-1.5Co-0.6Si alloy in Fig. 1 (a) is 66 ± 2 μm, while the dendrite spacing of the as-cast Cu-1.5Ni-1.5Co-0.6Si alloy is 78 ± 2 μm in Fig. 1(c). Additionally, the solid-solution optical microstructure of the Cu-1.5Ni-1.0Co-0.6Si and Cu-1.5Ni-0.6Si-Co alloys aged at 900 °C for 2 h is shown in Fig. 1(b), where the grain size is 74 ± 2 μm and in Fig. 1(d), where the grain size is 95 ± 2 μm. Increased addition of Co leads to coarser grain size during alloy casting and solid-solution treatment.

Table 1
Chemical composition of designed alloy (mass fraction, %).

Alloys	Ni	Co	Si	Cu
Cu-1.5Ni-1.0Co-0.6Si	1.5	1.0	0.6	Bal.
Cu-1.5Ni-1.5Co-0.6Si	1.5	1.5	0.6	Bal.

The cold rolled and solid solution samples were cut by the wire electrical discharge machining to the 100 mm × 10 mm × 5 mm size. The cold deformation was 0%, 40% and 80%, respectively. In order to clearly reflect alloy microstructure changes during cold deformation, the cold rolling model of the alloy was obtained by combining the optical microstructure with the Pro/E three-dimensional software modeling, as shown in Fig. 2, where some grains are elongated along the rolling direction. The cold deformation of the Cu-Ni-Co-Si alloy is under the recrystallization temperature. The deformation of the Cu-Ni-Co-Si alloy is calculated as:

$$\text{Deformation} = \frac{d_b - d_a}{d_b} \times 100\% \quad (1)$$

here, d_b (mm) is the thickness before the deformation and d_a (mm) is the thickness after deformation.

After 450 °C 2 h aging, the microstructure of the Cu-1.5Ni-1.0Co-0.6Si and Cu-1.5Ni-1.5Co-0.6Si alloys with 40% cold deformation is shown in Fig. 3(a) and Fig. 3(b), respectively. This indicates that the unsaturated solid solution formed by the alloy elements dissolved in the copper matrix, gradually precipitating and distributing evenly in the copper matrix.

3.2. Hardness and conductivity

The hardness and conductivity of the alloys after a different amount of cold deformation are shown in Fig. 4. Comparing the hardness of the Cu-1.5Ni-1.5Co-0.6Si and Cu-1.5Ni-1.0Co-0.6Si alloys in Fig. 4(a), it can be seen that the hardness increased with cold deformation. Similarly, the conductivity also increased in Fig. 4(b). It is observed that the Cu-1.5Ni-1.5Co-0.6Si alloy has a higher hardness at the same cold deformation, but lower electrical conductivity.

Fig. 5(a) and Fig. 5(b) show the hardness and conductivity of the Cu-1.5Ni-1.0Co-0.6Si alloy after solution treatment at 900 °C for 2 h and 40% cold deformation, followed by aging treatment at 400 °C, 450 °C, 500 °C, and 550 °C, respectively. Fig. 5(c) and (d) show the hardness and conductivity of the Cu-1.5Ni-1.5Co-0.6Si alloy under the same conditions as in Fig. 5(a) and (b). It can be seen that the hardness of the alloy initially increased rapidly and then decreased with aging time at a given temperature. Peak values of the Cu-1.5Ni-1.0Co-0.6Si alloy hardness were 230 HV aged at 400 °C for 240 min, 240 HV aged at 450 °C for 120 min, 250 HV aged at 500 °C

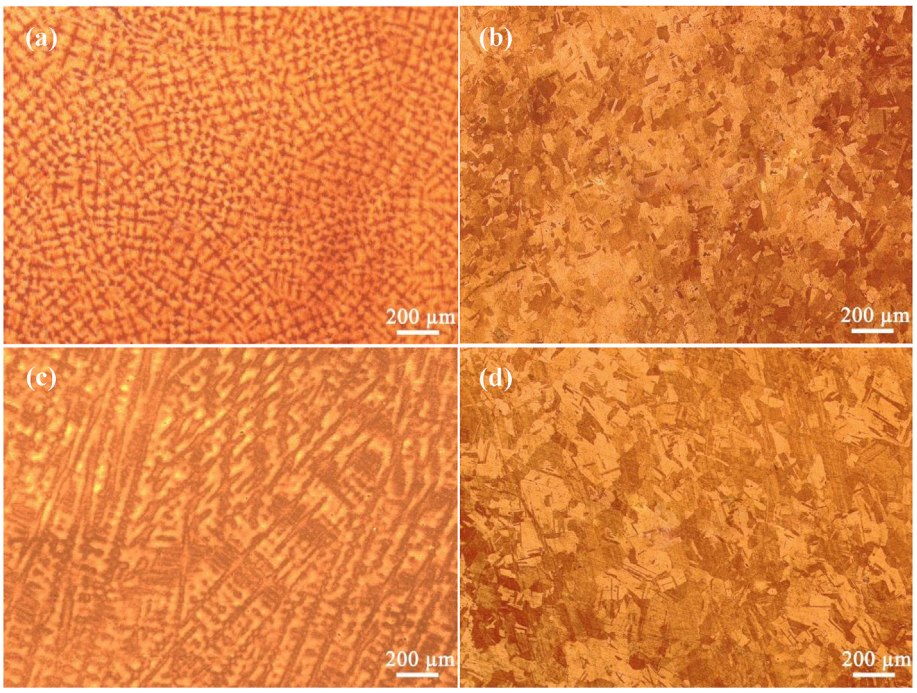

Fig. 1. Microstructure of: (a) as cast Cu-1.5Ni-1.0Co-0.6Si alloy; (b) solid-solution Cu-1.5Ni-1.0Co-0.6Si alloy; (c) as cast Cu-1.5Ni-1.5Co-0.6Si alloy; (d) solid-solution Cu-1.5Ni-1.5Co-0.6Si alloy.

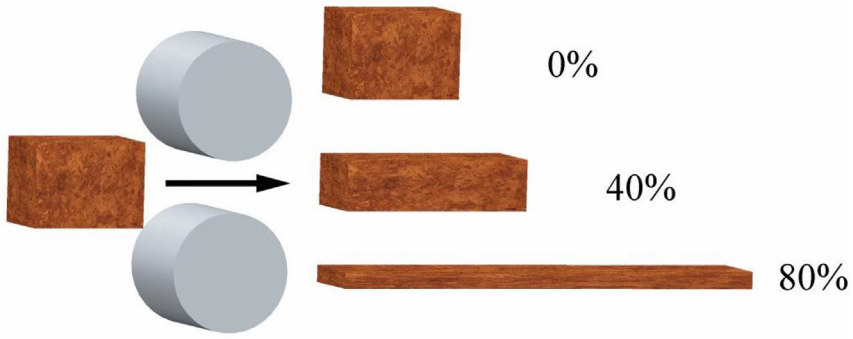

Fig. 2. Diagram of cold rolling with different deformations.

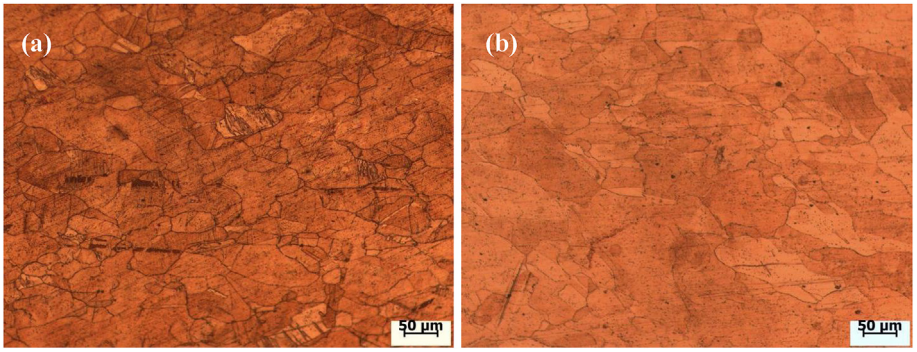

Fig. 3. Optical micrograph of designed Cu-Ni-Co-Si alloys after cold-rolled by 40% and aged at 450 °C for 2 h. (a) Cu-1.5Ni-1.0Co-0.6Si alloy; (b) Cu-1.5Ni-1.5Co-0.6Si alloy.

for 60 min, and 238 HV aged at 550 °C for 30 min. The corresponding conductivity values were 36% IACS, 40% IACS, 43% IACS, and 44% IACS, respectively. The peak values of the Cu-1.5Ni-1.5Co-0.6Si alloy hardness were 244 HV aged at 450 °C for 120 min, 236 HV aged at 500 °C for 60 min, and 233 HV aged at 550 °C for 30 min. Meanwhile, the corresponding conductivity values were 35% IACS, 36% IACS, 35% IACS and 40% IACS, respectively. However, the hardness of the Cu-1.5Ni-1.5Co-0.6Si alloy continued to increase at

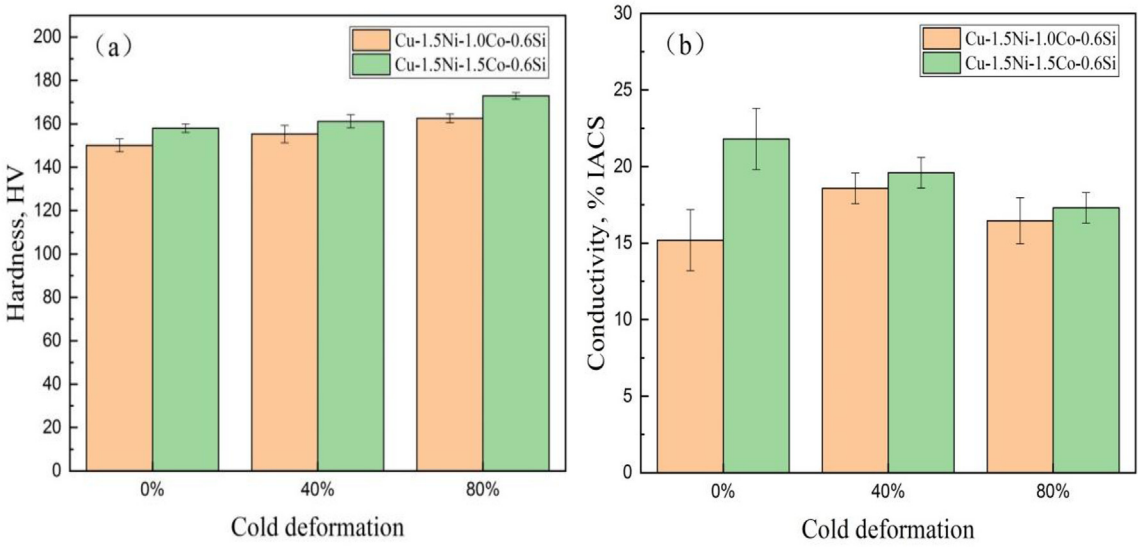

Fig. 4. (a) The hardness and (b) conductivity of the alloys at 0%, 40% and 80% deformation.

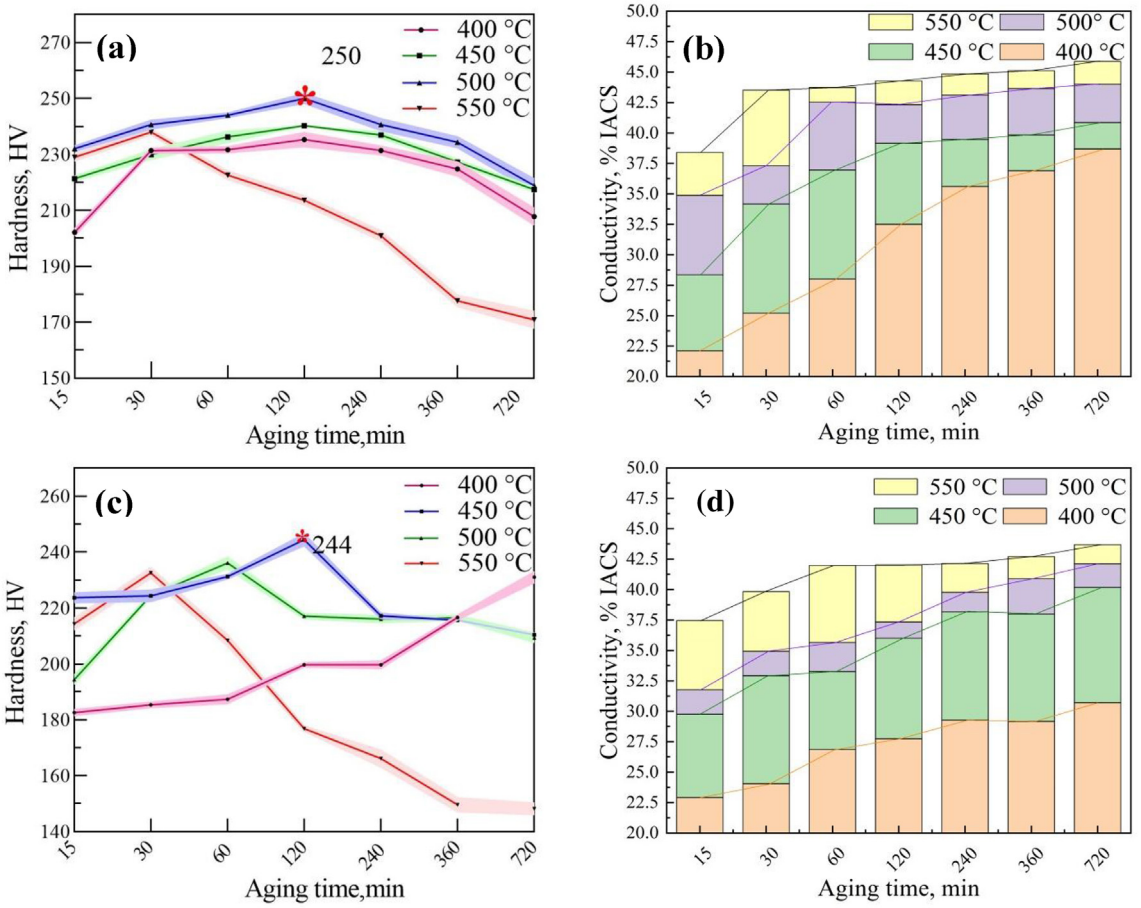

Fig. 5. (a, c) Hardness and (b, d) conductivity of the two alloys aged at different temperatures and time with 40% deformation.

400 °C aging.

It can be seen from Fig. 5(a) and (c) that the hardness of the two alloys initially increased rapidly until the peak value and then decreased with aging time at a given temperature, except the 400 °C aging curve in Fig. 5(c). The reason is because precipitates rapidly and massively separate out from the alloy in the early stages of aging, pin dislocations and strengthen the alloy, leading to the hardness increase until the peak value. With overaging, the hardness gradually decreased and became stable. In Fig. 5(c) the hardness of the Cu-1.5Ni-1.5Co-0.6Si alloy increased with aging time for

the alloy aged at 400 °C. This is due to the low aging temperature, which is not high enough for rapid atomic diffusion, leading to less precipitation and slower precipitation rate. This also means that the effect of pinning dislocation strengthening is not fully developed for the alloy. As mentioned above, the hardness of the alloy increases slowly. In addition, the higher the aging temperature, the lower the peak hardness value and much shorter aging time to the peak hardness value. The increase of temperature provided phase transformation driving force for precipitation of the alloy, leading to much faster precipitation, and even more obvious strengthening effect. Meanwhile, it is easy for the solute atoms to diffuse according to the formation of dislocations during the 40% cold deformation of the alloy, thus the hardness increases rapidly to reach the peak value in a short time. The conductivity of two alloys increases rapidly at first and then tends to stay stable with aging time in Fig. 5(b) and (d), where the higher the temperature, the higher the conductivity and the faster the stable value is attained. The reason is that precipitates separate out rapidly and massively from the alloy in the early stages of aging. The Cu alloy matrix tends to become more pure and thus the conductivity increases. However, the conductivity tends to be stable as the secondary phases precipitated slowly from the matrix with prolonged aging time [25,26]. The high temperature increased the precipitation rate and the rate of matrix purification, leading to a fast increase in conductivity.

Fig. 6(a), (c) show the hardness and (b), (d) conductivity curves of the two alloys aged at 450 °C for different cold deformation to aging. Both the hardness and conductivity of the two alloys increased with deformation. The peak hardness of the Cu-1.5Ni-1.0Co-0.6Si alloy increases with the cold deformation, reaching 234, 239, and 244 HV with 0%, 40%, and 80% cold rolling, respectively, in Fig. 6(a). The dislocations with cold deformation play a role of providing a diffusion path for the solute atoms, along with the nucleation sites during aging. The higher peak hardness depends on the higher cold deformation. The conductivity curves of the two alloys are shown in Fig. 6(b) and (d), respectively. They indicate that rolling leads to higher conductivity at a given aging time. Cold deformation can cause crystal defects, such as vacancies and dislocations in the alloy, improve lattice distortion energy, and increase the amount of the precipitation phase, improving the alloy conductivity [27–29].

After 40% cold rolling and 450 °C aging for 120 min, the hardness of the Cu-1.5Ni-1.0Co-0.6Si and Cu-1.5Ni-1.5Co-0.6Si alloys reached the peak values (240 HV and 244 HV with 39% IACS and 36% IACS corresponding conductivity, respectively), and then decreased slightly with aging time. Compared with the Cu-1.5Ni-1.0Co-0.6Si alloy, the hardness and conductivity of the Cu-1.5Ni-1.5Co-0.6Si alloy decreased slightly after cold deformation and aging, as shown in Figs. 5 and 6. This means that the size and distribution of precipitates, and the morphology of the precipitates have strong effects on the hardness and conductivity, which will be discussed according to the X-ray diffraction analysis and TEM.

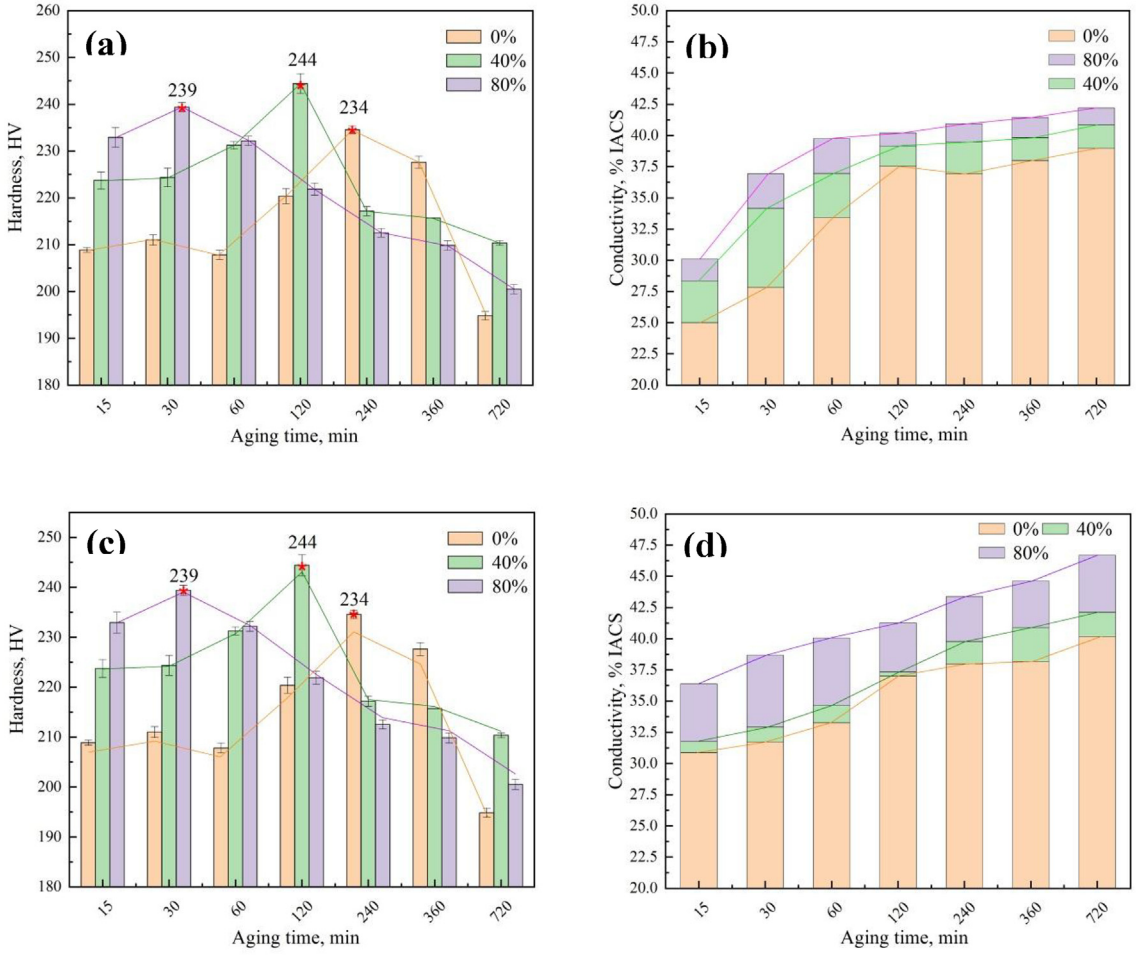

Fig. 6. (a, c) Hardness and (b, d) conductivity of the two alloys aged at 450 °C with different deformation.

3.3. Precipitates

Fig. 7 shows the structure of the precipitate in the Cu-Ni-Si-Co alloy. Ni and Si can form the Ni_3Si and Ni_2Si phases, while Co and Si can form the Co_2Si. The corresponding crystal structures are shown in Fig. 7(a), (b) and (c), respectively. Ni_3Si has a simple cubic structure with the lattice parameter a = 0.351 nm, *Pm*-3m (221) [30]. Ni_2Si and Co_2Si phases have the same structure and very similar lattice parameters: Ni_2Si has orthorhombic structure, a = 0.706 nm, b = 0.499 nm and c = 0.372 nm, Pbnm (62) [31], while the lattice parameter in Co_2Si is a = 0.0.710 nm, b = 0.491 nm, and c = 0.378 nm [32].

Fig. 8 displays HRTEM micrographs and selected-area diffraction patterns (SADPs) of Cu-1.5Ni-1.0Co-0.6Si after 40% cold deformation, and then aged at 450 °C for 2 h. The selected-area electron diffraction patterns demonstrate that precipitates with three different shapes can be clearly seen in Fig. 8. In Fig. 8(a) two different precipitated phases are found, one is large precipitate with the size of 248 nm and the others are finely dispersed precipitates. According to the SADP of the large precipitation phase in Fig. 8(b), the large precipitate is Co_2Si, and has an orthogonal structure, similar to δ-Ni_2Si. Fig. 8(c) shows the XRD of the fine precipitates in Fig. 8(b).

The selected-area electron diffraction pattern shows precipitates with three different shapes in Fig. 8(d), which are disc-shaped, rod-shaped and small bulks, respectively. Jia et al. have found that the shape of the δ-Ni_2Si is disc-shaped, however, the shape of δ-Ni_2Si changed to rod-shaped when parallel to the beam [33]. According to Refs. [23,24,34], Co can replace Ni and form precipitates of $(Ni, Co)_2Si$ in the Cu-Ni-Si-Co alloy. XRD results show large amounts of Ni, Co, and Si elements in the alloy, which can not conform to the atomic ratio of δ-Ni_2Si and β-Ni_3Si. Thus, it can be considered that there is not a single δ-Ni_2Si phase in the Cu-1.5Ni-1.0Co-0.6Si alloy, but $(Ni, Co)_2Si$ and β-Ni_3Si. Meanwhile, it can be considered that $(Ni, Co)_2Si$ also has different orientations due to the δ-Ni_2Si having different orientations. The SADP along [001] Cu in Fig. 8(d) is shown in Fig. 8(e). The diffraction patterns of $(Ni, Co)_2Si$ and β-Ni_3Si in Fig. 8(d) are superimposed on each other to form a composite SADP in Fig. 8(e). The above results were also verified by Fig. 8(f). From Fig. 8(e), the crystal orientation relationship between the copper matrix and precipitates (β-Ni_3Si, subscript represents the orientation of $(Co, Ni)_2Si$ precipitates), has been determined as:

$$[001]Cu//[001]\beta//\ [001]p,\ (220)Cu//\ (110)\beta//\ (100)p$$

Fig. 9 shows the TEM (HRTEM) micrographs and SADPs of the Cu-1.5Ni-1.0Co-0.6Si alloy cold rolled with 40% and aged at 450 °C for 12 h. Fig. 8(a) shows dislocations and precipitation, with SADP and HRTEM is Fig. 9(b) and (c), respectively. Fig. 9(d) is the selected-area dark-field micrograph of Fig. 9(a), and the corresponding SADP and HRTEM are shown in Fig. 9(e) and (f). The microstructure of 450 °C aged for 2 h and 12 h was observed by TEM in Figs. 8 and 9. The three phases in the Cu-1.5Ni-1.0Co-0.6Si alloy were found,

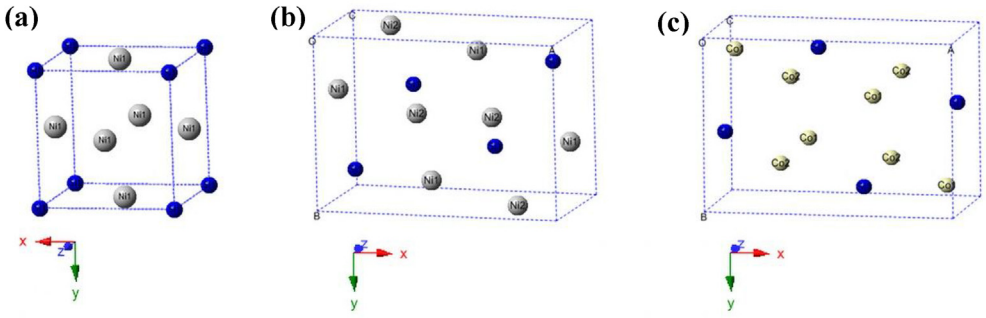

Fig. 7. Schematics of the precipitates crystal structure: (a) β-Ni_3Si with L12 ordering; (b) δ-Ni_2Si, and (c) Co_2Si.

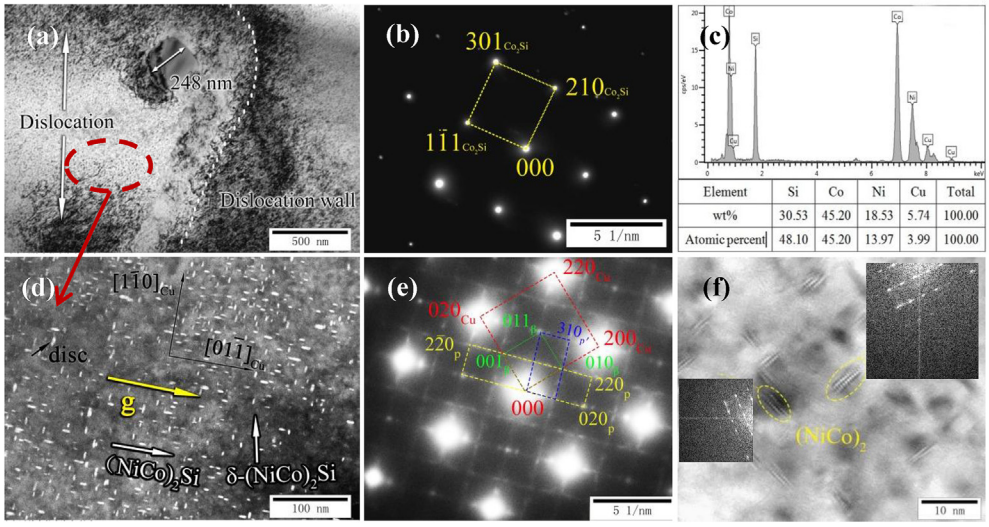

Fig. 8. HRTEM micrographs and selected-area diffraction patterns (SADPs) of the Cu-1.5Ni-1.0Co-0.6Si alloy cold rolled by 40% and aged at 450 °C for 2 h: (a) Selected-area dark-field micrograph; (b) SADP along [001] Cu of (a); (c) XRD analysis of (a); (d) TEM of (a); (e) SADP of the large precipitation phase of (d); (f) SADP and HRTEM of (d).

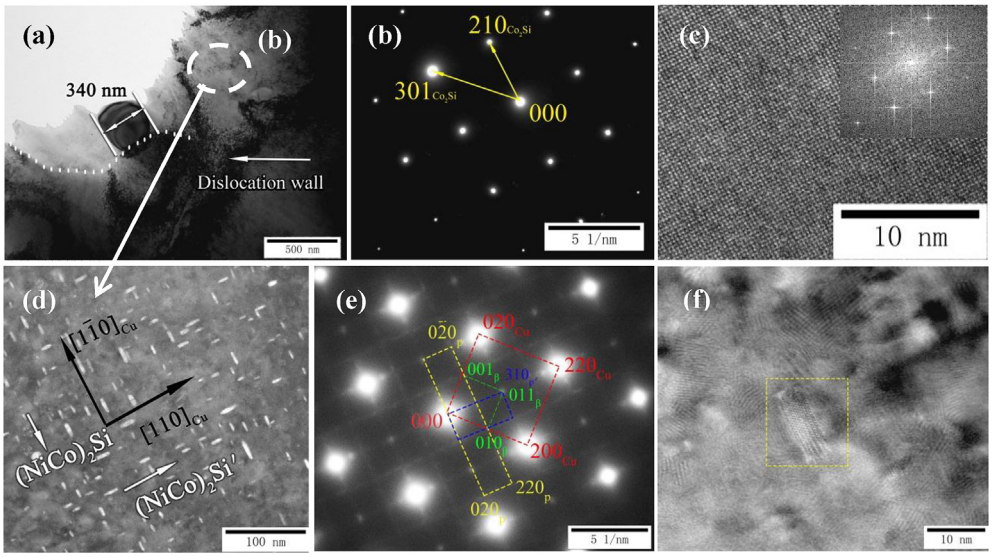

Fig. 9. HRTEM micrographs and selected-area diffraction patterns (SADP) of the Cu-1.5Ni-1.0Co-0.6Si alloy cold rolled by 40% and aged at 450 °C for 12 h: (a) selected-area dark-field micrograph showing dislocation wall; (b) SADP along [001] Cu of (a); (c) HRTEM of (a); (d) Precipitates of (a); (e) SADP of the large precipitation phase in (d); (f) HRTEM of the large precipitation phase in (d).

which are fine (Ni, Co)$_2$Si and β-Ni$_3$Si phases, and the coarse Co$_2$Si with the average size of 250 nm. It can be seen that the same precipitation characteristics were obtained whether the alloy was aged for 12 h or 2 h. The difference is that the average grain size of the precipitated phase increased with 12 h aging. For example, the (Ni, Co)$_2$Si phase grew from 7 nm in Fig. 8(d) to 15 nm in Figs. 8(f) and 9(c), and the coarse Co$_2$Si phase grew from 248 nm in Fig. 8(a) up to 340 nm in Fig. 9(a).

The homogeneous precipitation occurs in the sub-grain of the alloy, which is divided by dislocation cell walls during 2 h aging. A large amount of fine and dispersed (Ni, Co)$_2$Si precipitated, resulting in intense age hardening of the alloy and increased strength of the alloy. The peak hardness of the Cu-1.5Ni-1.0Co-0.6Si alloy reached 250 HV after aging for 2 h at 450 °C. It can be seen that the overaging appeared after 2 h aging, which can reduce the alloy hardness, as shown in Fig. 5. Cu-1.5Ni-1.0Co-0.6Si alloy contains a mass of silicide-forming elements, which are Ni and Co. The silicide compound can effectively promote age hardening, inhibit grain growth and improve softening resistance. It was shown that the dislocations in Figs. 8(a) and 9(a) are multiplied, slip, annihilate and recombine to form dislocation walls. The dislocation walls and groups hinder the large Co$_2$Si precipitated phase from moving, and it was also confirmed that the secondary precipitation phase can effectively pin dislocations. The coarse Co$_2$Si phase in Figs. 8(a) and 9(a) was analyzed and it was calculated that the Co$_2$Si habit plane is {331}.

The Cu-1.5Ni-1.5Co-0.6Si alloy aged at 450 °C for 2 h after 40% cold rolling deformation has the same precipitates, and similar TEM micrographs are shown in Fig. 10. Compared with the Cu-1.5Ni-1.5Co-0.6Si alloy, the increased Co content from 1.0 wt% to 1.5 wt % resulted in larger average precipitates size of 10 nm in Fig. 10(a). The HRTEM of Fig. 10(a) is shown in Fig. 10(b), which also indicated that the precipitate is (Ni, Co)$_2$Si. In Fig. 10(c), the dislocations and precipitates are shown, and the average size of Co$_2$Si is 340 nm. The corresponding SADP and HRTEM are shown in Fig. 10(d).

Based on the analysis of hardness and conductivity, it is inferred that the properties of Cu-1.5Ni-1.5Co-0.6Si alloy are inferior to Cu-1.5Ni-1.0Co-0.6Si due to the addition of the excessive Co amount, which changed the precipitated phase size in the Cu-1.5Ni-0.6Si alloy. Comparing the TEM structures of the two alloys in the same state in Figs. 8 and 10, it can be found that the Cu-1.5Ni-1.5Co-0.6Si and Cu-1.5Ni-1.0Co-0.6Si alloys have the same precipitation phases. With the Co content increase from 1.0 wt% to 1.5 wt% in the Cu-1.5Ni-0.6Si alloy, the size of (Ni, Co)$_2$Si and Co$_2$Si precipitated phases increased slightly to 7–10 nm. In addition, Co and Ni compete for the Si element due to the (Ni, Co)$_2$Si and Co$_2$Si phases forming at the same time. It can be concluded that the surplus Co and Ni are formed and dissolved in the alloy matrix, resulting in slightly degraded properties of the Cu-1.5Ni-1.5Co-0.6Si alloy compared with Cu-1.5Ni-1.0Co-0.6Si. The peak hardness of the Cu-1.5Ni-1.0Co-0.6Si alloy aged at 450 °C for 2 h is 250 HV and 36% IACS, while for the Cu-1.5Ni-1.5Co-0.6Si alloy the corresponding values are 244 HV and 35% IACS.

The microstructure observations of the Cu-1.5Ni-1.0Co-0.6Si alloy aged at 450 °C for 2 h in Fig. 10 indicate that a large number of fine and uniform disc precipitates, which have a certain preferred orientation, are distributed in the Cu matrix. According to the analysis mentioned in Fig. 8, the surface of the disk precipitates is not necessarily parallel to the incident direction of the electron beam. Therefore, the width of the precipitate is shown in Fig. 10(a) and (b) (dark-flied image of Fig. 10(a)), which is not necessarily equal to its thickness, but it can be considered that the width must be greater than the thickness.

The diffraction pattern and HRTEM of Fig. 10(a) are shown respectively in Fig. 10(c) and (d), where the incident direction of the electron beam is approximately parallel to the crystal orientation of the substrate <112>Cu. It was found that the precipitates in the Cu-1.5Ni-1.0Co-0.6Si alloy have the orthorhombic structure, which is similar to the precipitates in Fig. 7(d). Thus, it also can be considered that the precipitated phase is (Co, Ni)$_2$Si. In addition, the β-Ni$_3$Si phase is also present in Fig. 10(c). The corresponding crystal orientation relationship between the copper matrix and the precipitates has been determined as:

$$[112]\mathrm{Cu}//[112]\beta//[012]\mathrm{p},\ (1\bar{1}1)\mathrm{Cu}//(1\bar{1}1)\beta//(021)\mathrm{p}$$

Fig. 12(a) and Fig. 11 (b) show a clear twin structure with uniformly distributed precipitates around and inside. Fig. 12(b) shows that the precipitates are distributed inside the twins. Meanwhile, the corresponding diffraction pattern is shown in Fig. 12(c), where

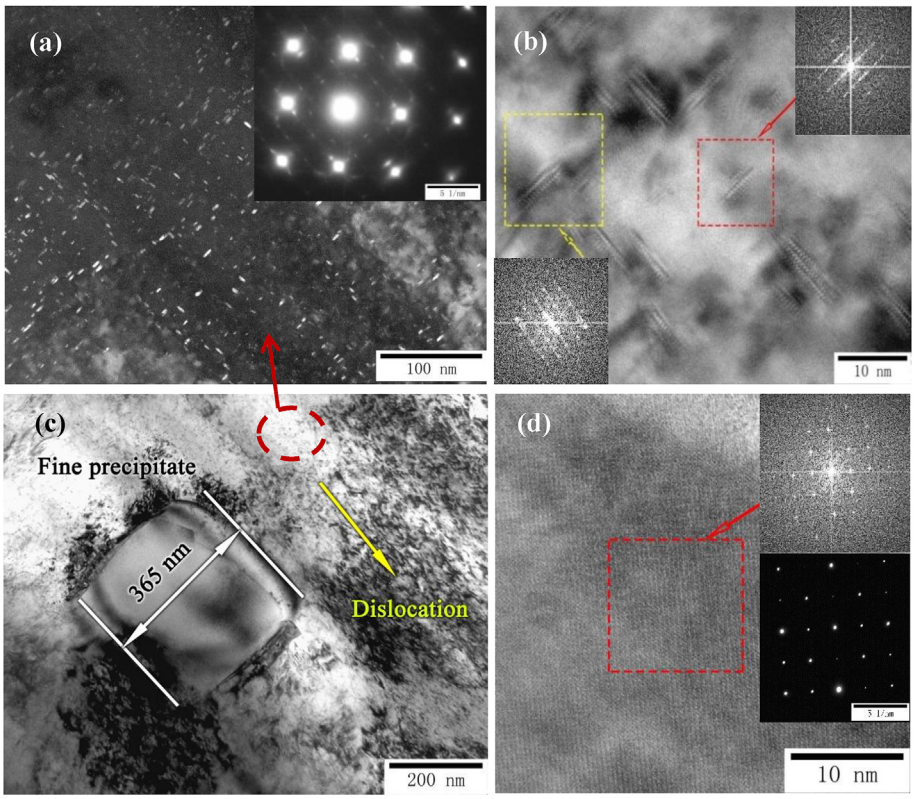

Fig. 10. HRTEM micrographs and selected-area diffraction patterns (SADP) of the Cu-1.5Ni-1.5Co-0.6Si alloy: (a) selected-area bright-field micrograph and SADP along [001] Cu of (c); (b) HRTEM of (a); (c) Dislocations and precipitates; (d) SADP and HRTEM are the large precipitation phase in (d).

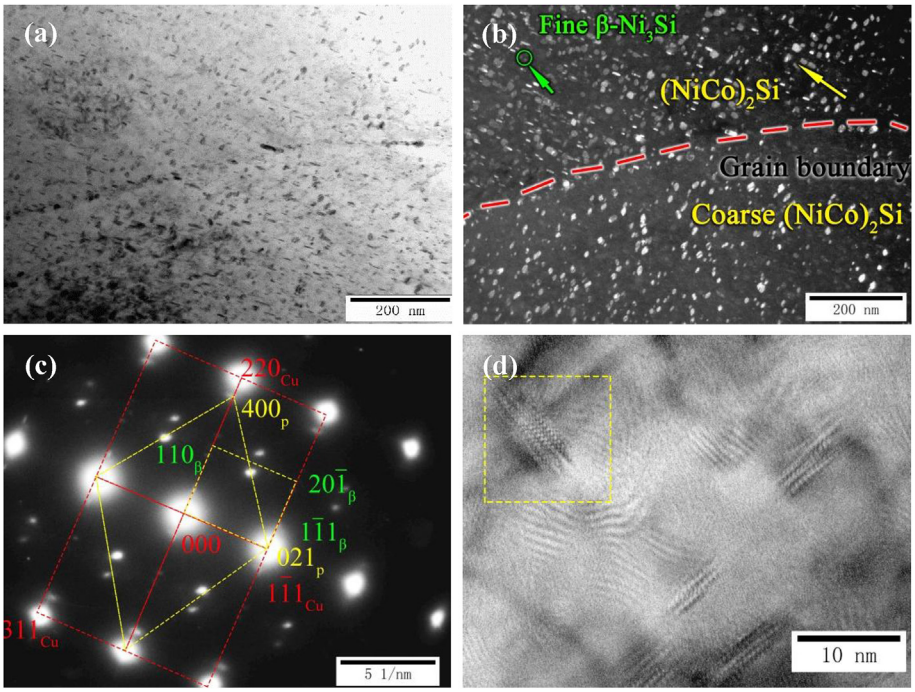

Fig. 11. HRTEM and selected-area diffraction patterns (SADP) of the Cu-1.5Ni-1.0Co-0.6Si alloy aged at 450 °C for 2 h: (a) Dark-flied; (b) bright-flied of (a); (c) SADP of (a), beam direction along [112] Cu; (d) HRTEM of (a).

the precipitates are β-Ni_3Si. Fig. 12(d) also shows the distribution of the β-Ni_3Si phase, and the diffraction pattern is shown in Fig. 12(e). Fig. 12(f) showed that a typical dislocation bypass mechanism was observed. At the same time, the precipitates and dislocations in the twins (marked by the red line) also showed the same dislocation bypass mechanism. A clear interaction between the precipitates

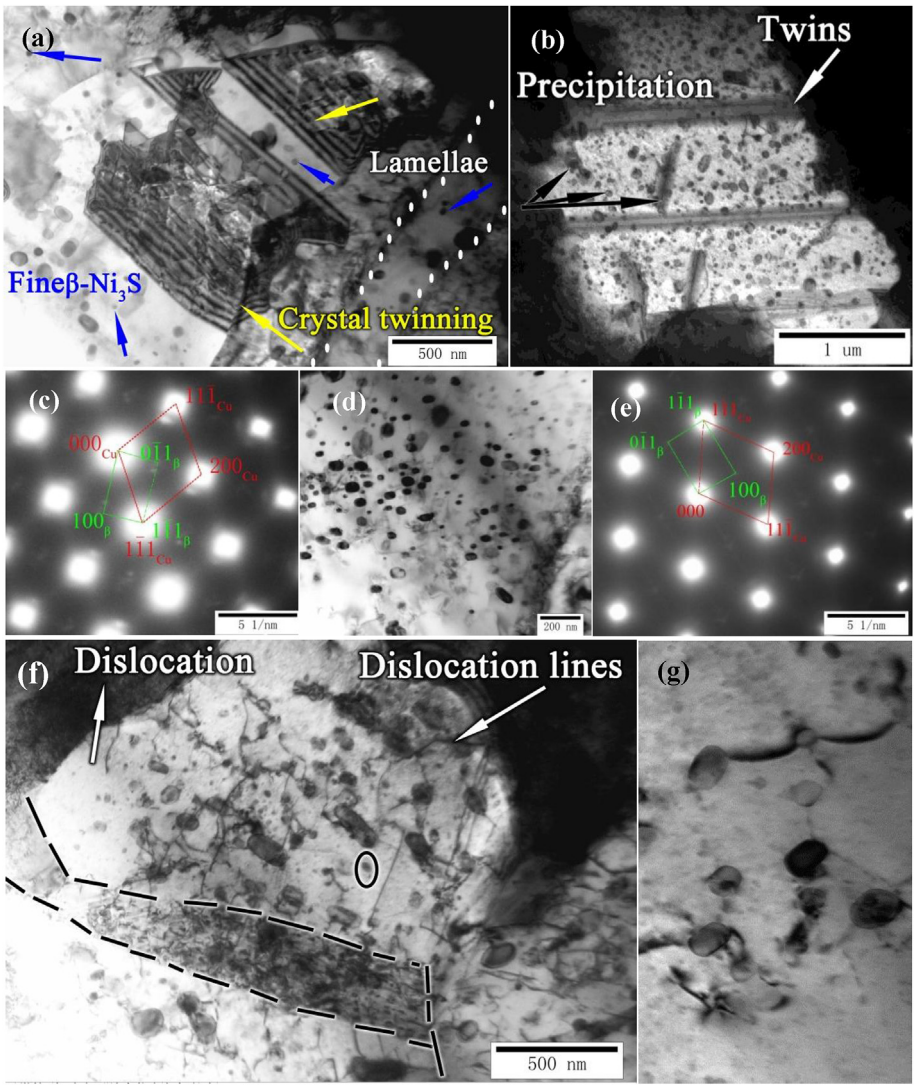

Fig. 12. TEM micrographs and selected-area diffraction patterns (SADP) belong to (011) Cu of the Cu-1.5Ni-1.0Co-0.6Si alloy aged at 450 °C for 2 h: (a) and (b) Selected-area dark-field micrograph showing twin structure and precipitates; (c) SADP of (a); (d) The other selected-area dark-field micrograph showing precipitates; (e) SADP of (d); (f) dislocation and precipitates; (g) TEM microphotograph of (f).

and dislocations was observed in Fig. 12(g). This indicated that the dislocation bypass mechanism plays an important role in strengthening the alloys. Additionally, the twin mechanism also plays an important role. The lamella structure was also observed in Fig. 12(a) (marked by the red line). At the early stage of aging, there is not enough time for the supersaturated solid solution alloy to continue aging at 450 °C. Finally, the interactions between the precipitation recrystallization processes resulted in this structure.

4. Discussion

4.1. Phase transformation behavior

Many reports of the phase transitions in the Cu-Ni-Si alloy noticed the different orientation relationships (OR) of the crystals in the past few decades. The Cu-Ni-Si alloy phase transformations can change with aging temperature and time. Jia et al. studied the phase transition of the Cu-1.5Ni-0.34Si alloy at 450 °C aging, where the supersaturated solid solution is decomposed into δ-Ni_2Si. The δ-Ni_2Si was formed on the (100) face of the δ-Ni_2Si phase with the Bain orientation relationship, so that the evolution of the orientation relationship between δ-Ni_2Si and the copper matrix is: Bain OR→ quasi N-W OR→ quasi K-S OR [34]. Xiao et al. believe that the phase change order in the Cu-1.4Ni-1.2Co-0.6Si alloy does not have a series of metastable processes (spinodal decomposition), but directly forms the stable (Ni, Co)$_2$Si phase [35], and the addition of some Co inhibits spinodal decomposition.

Spinodal decomposition is a typical phase transformation during the aging process in the Cu-Ni-Si alloy, which decreases the conductivity of the alloy. The microstructure of the alloy aged at 450 °C for 2 h was analyzed by TEM. The similar microstructure and the same SADP can be clearly seen in the Cu-1.5Ni-1.0Co-0.6Si and Cu-1.5Ni-1.5Co-0.6Si alloys. The SADP shows that there are four phases in the aging process of the alloy: FCC matrix, (Ni, Co)$_2$Si precipitation, β-Ni_3Si, and Co_2Si. The crystal orientation relationship between the matrix and precipitates of the (Ni, Co)$_2$Si and β-Ni_3Si is: [112]Cu//[112]β//[012]p, $(1\bar{1}1)$Cu//$(1\bar{1}1)$β//(021)p; [001]Cu//[001]β//[001]p, (220)Cu//(110)β//(100)p. The bright field images and selected-area diffraction patterns show that the typical spinodal decomposition cannot be found in the Cu-Ni-Co-Si alloy. Based on the TEM results and previous reports, the phase transition

Table 2
The values used for the calculation of the Orowan hardening of the alloy.

The designed alloy	f_v, %	dp, nm	v	G, GPa	b, nm	M	$\Delta\sigma_{Orowan}$, MPa
Cu-1.5Ni-1.0Co-0.6Si	0.03	7	0.34	48	0.255	3.1	495
Cu-1.5Ni-1.0Co-0.6Si	0.03	10	0.34	48	0.255	3.1	383

reaction for Cu-1.5Ni-0.6Si-(Co) during 450 °C aging is: supersaturated solid solution→ (Ni, Co)$_2$Si precipitation + β-Ni$_3$Si + Large Co$_2$Si.

4.2. Strengthening mechanisms

The high strength of the studied Cu-Ni-Co-Si alloy can be explained by the four strengthening mechanisms: precipitation strengthening, sub-structure strengthening, solid solution strengthening, and dislocation strengthening. The main strengthening mechanism is the precipitation hardening based on dislocation interaction with nano-scale precipitates. It can be expressed by the Orowan-Ashby equation [36–39]:

$$\tau_{precip.} = \frac{0.81Gb}{2\pi(1-\nu)^{1/2}} \bullet \frac{\ln\left(d_{precip.}/b\right)}{(\lambda - d_{precip.})} \quad (2)$$

where G is the shear modulus of the matrix, $d_{precip.}$ is the average diameter of the particles (the value is measured from ten or more TEM images), b is the Burgers vector, ν is the Poisson's ratio, and λ is the spacing between particles in the glide plane. This spacing is related to the radius, $d_{precip.}$, and the volume fraction fv of the secondary phase particles (mass divided by density), expressed as [40,41]:

$$\lambda = \frac{1}{2} d_{precip.} \sqrt{\frac{3\pi}{2f\nu}} \quad (3)$$

The Orowan mechanism can be expressed as:

$$\Delta\sigma_{\mathrm{Orowan}} = M \bullet \tau_{precip.} \quad (4)$$

Here, M is the Taylor factor for the copper alloy. We only considered the yield strength change caused by the nano-scale (Ni, Co)$_2$Si for simplifying the calculation of fv, as it is assumed that Si and Co atoms are completely precipitated in the form of nano-scale (Ni, Co)$_2$Si particles in the alloy treated with the final aging temperature of 450 °C for 2 h. The calculated results are listed in Table 2.

The Cu-1.5Ni-1.0Co-0.6Si and Cu-1.5Ni-1.5Co-0.6Si alloys have the same precipitated structure. It is noteworthy that the average size of the precipitated phase in the Cu-1.5Ni-1.0Co-0.6Si alloy is finer than in the Cu-1.5Ni-1.5Co-0.6Si alloy. For example, the average size of (Ni, Co)$_2$Si in the Cu-1.5Ni-1.0Co-0.6Si and Cu-1.5Ni-1.5Co-0.6Si alloys aged at 450 °C for 2 h is 7 nm and 10 nm, respectively. It can be concluded that (Ni, Co)$_2$Si and Co$_2$Si are formed at the same time during aging. Co and Ni compete for the Si element. Thus, the Cu-1.5Ni-1.5Co-0.6Si alloy has surplus Co and Ni, which dissolved in the alloy matrix to reduce the alloy's comprehensive performance.

5. Conclusions

The microstructure evolution and properties of the Cu-1.5Ni-0.6Si-(Co) alloy were investigated in this work. The main conclusions can be summarized as follows:

(1) Cu-1.5Ni-0.6Si-(Co) alloy has three precipitated phases, which are (Ni, Co)$_2$Si + β-Ni$_3$Si + Large Co$_2$Si formed during the aging process. Some nickel atoms are substituted to form the (Ni, Co)$_2$Si phase, which grows in size with the increase of Co content from 1.0 wt% to 1.5 wt%.
(2) The crystal orientation relationship between the matrix and precipitates of (Ni, Co)$_2$Si and β-Ni$_3$Si is: [112]Cu//[112]β//[012]p, $(1\bar{1}1)$Cu//$(1\bar{1}1)\beta$//(021)p, [001]Cu//[001]β//[001]p, (220)Cu//(110)β//(100)p.
(3) The Co content increase from 1.0 wt% to 1.5 wt% leads to degraded physical properties of the alloy. It also changed the microstructure of the alloy, promoted the growth of the precipitates, and accelerated precipitation during the aging process. The hardness and conductivity of the Cu-1.5Ni-1.0Co-0.6Si alloy with 40% deformation aged at 500 °C for 2 h are 250 HV and 43% IACS, respectively.

Acknowledgments

This work was supported by the Open Cooperation Project of Science and Technology of the Henan Province (182106000018), the Henan University Scientific and Technological Innovation Talent Support Program (18HASTIT024) and the National Natural Science Foundation of China (U1704143).

References

[1] Z.J. Zhang, P. Zhang, Z.F. Zhang, Cyclic softening behaviors of ultra-fine grained Cu-Zn alloys, Acta Mater. 121 (1) (2016) 331–342.
[2] J.Y. Cheng, B.B. Tang, F.X. Yu, Evaluation of nanoscaled precipitates in a Cu-Ni-Si-Cr alloy during aging, J. Alloys Compd. 614 (25) (2014) 189–195.
[3] M. Hatakeyama, T. Toyama, Y. Nagai, M. Hasegawa, M. Eldrup, B.N. Singh, Nanostructural evolution of Cr-rich precipitates in a Cu-Cr-Zr alloy during heat treatment studied by 3 dimensional atom probe, Mater. Trans. 49 (3) (2008) 518–521.
[4] K. Lu, L. Lu, S. Suresh, Strengthening materials by engineering coherent internal boundaries at the nanoscale, Science 324 (4) (2009) 349–352.
[5] W.A. Soffa, D.E. Laughlin, High-strength age hardening copper–titanium alloys: redivivus, Prog. Mater. Sci. 49 (3–4) (2004) 347–366.
[6] L. Lu, X. Chen, X. Huang, K. Lu, Revealing the maximum strength in nanotwinned copper, Science 323 (1) (2009) 607–610.
[7] X.Z. Zhou, Y.C. Su, A novel Cu-Ni-Zn-Al alloy with high strength through precipitation hardening, Mater. Sci. Eng. A 527 (20) (2010) 5153–5156.
[8] D.P. Lu, J. Wang, W.J. Zeng, Y. Liu, L. Lu, B.D. Sun, Study on high-strength and high-conductivity Cu-Fe-P alloys, Mater. Sci. Eng. A 421 (1-2) (2006) 254–259.
[9] Q. Lei, Z. Li, J. Wang, J.M. Xie, X. Chen, S. Li, Y. Gao, L. Li, Hot working behavior of a super high strength Cu-Ni-Si alloy, Mater. Des. 51 (10) (2013) 1104–1109.
[10] Q. Lei, Z. Li, L. Han, Z. Xiao, T. Xiao, Effect of aging time on the corrosion behavior of a Cu-Ni-Si alloy in 3.5wt% NaCl solution, Corrosion 72 (5) (2016) 615–627.
[11] Y. Zhang, A.A. Volinsky, H. Tran, Z. Chai, P. Liu, B.H. Tian, Y. Liu, Aging behavior and precipitates analysis of the Cu-Cr-Zr-Ce alloy, Mater. Sci. Eng. A 650 (1) (2016) 248–253.
[12] Q. Lei, Z. Li, T. Xiao, Y. Pang, Z.Q. Xiang, W.T. Qiu, Z. Xiao, A new ultrahigh strength Cu-Ni-Si alloys, Intermetallics 42 (12) (2013) 77–84.
[13] H. Wang, L.K. Gong, J.F. Liao, H.M. Chen, W.B. Xie, B. Yang, Restraining metastable fcc-Cr phase by restraining nucleation of equilibrium bcc-Cr phase in CuCrZrTi alloys during ageing, J. Alloys Compd. 749 (15) (2018) 140–145.
[14] B.J. Wang, Y. Zhang, B.H. Tian, V. Yakubov, J.C. An, A.A. Volinsky, Y. Liu, K.X. Song, L.H. Li, M. Fu, Effects of Ce and Y addition on microstructure evolution and precipitation of Cu-Mg alloy hot deformation, J. Alloys Compd. 781 (4) (2019) 118–130.
[15] Q. Lei, Z. Li, J. Wang, S. Li, L. Zhang, Q.Y. Dong, High-temperature deformation behavior of Cu-6.0Ni-1.0Si-0.5Al-0.15Mg-0.1Cr alloy, Mater. Sci. 47 (16) (2012) 6034–6042.
[16] Z. Li, Z.Y. Pan, Y.Y. Zhao, Z. Xiao, M.P. Wang, Microstructure and properties of high conductivity, super high strength Cu-8.0Ni-1.8Si-0.6Sn-0.15Mg alloy,

Mater. Res. 24 (6) (2009) 2123–2129.
[17] H.S. Wang, H.G. Chen, J.W. Gu, C.E. Hsu, C.Y. Wu, Improvement in strength and thermal conductivity of powder metallurgy produced Cu-Ni-Si-Cr alloy by adjusting Ni/Si weight ratio and hot forging, J. Alloys Compd. 633 (5) (2015) 59–64.
[18] W. Wang, H.J. Kang, Z.N. Chen, Z.J. Chen, C.L. Zou, R.G. Li, G.M. Yin, T.M. Wang, Effects of Cr and Zr additions on microstructure and properties of Cu-Ni-Si alloys, Mater. Sci. Eng. A 673 (15) (2016) 378–390.
[19] V.T. Witusiewicz, I. Arpshofen, H.J. Seifert, F. Sommer, F. Aldinger, Enthalpy of mixing of liquid and undercooled liquid ternary and quaternary Cu-Ni-Si-Zr alloys, J. Alloys Compd. 337 (1–2) (2002) 155–167.
[20] X.P. Xiao, B.Q. Xiong, Q.S. Wang, G.L. Xie, L.J. Peng, G.H. Huang, Microstructure and properties of Cu-Ni-Si-Zr alloy after thermomechanical treatments, Rare Met. 32 (2) (2013) 144–149.
[21] Y. Zhang, A.A. Volinsky, Q.Q. Xu, Z. Chai, B.H. Tian, P. Liu, H.T. Tran, Deformation behavior and microstructure evolution of the Cu-2Ni-0.5 Si-0.15 Ag alloy during hot compression, Metall. Mater. Trans. 46 (12) (2015) 5871–5876.
[22] S.C. Krishna, J. Srinath, A.K. Jha, B. Pant, S.C. Sharma, K.M. George, Microstructure and properties of a high-strength Cu-Ni-Si-Co-Zr alloy, J. Mater. Eng. Perform. 22 (7) (2013) 2115–2120.
[23] J.Z. Huang, Z. Xiao, J. Dai, Z. Li, H. Jiang, W. Wang, X. Zhang, Microstructure and properties of a novel Cu-Ni-Co-Si-Mg alloy with super-high strength and conductivity, Mater. Sci. Eng. A 744 (28) (2019) 754–763.
[24] A. Ozawa, C. Watanabe, R. Monzen, Influence of Co on strength of Cu-Ni-Co-Si alloy, Mater. Sci. Forum (2014) 783–786.
[25] D.M. Zhao, Q.M. Dong, P. Liu, B.X. Kang, J.L. Huang, Z.H. Jin, Structure and strength of the age hardened Cu-Ni-Si alloy, Mater. Chem. Phys. 79 (1) (2003) 81–86.
[26] Y. Zhang, B.H. Tian, A.A. Volinsky, H.L. Sun, Z. Chai, P. Liu, X.H. Chen, Y. Liu, Microstructure and precipitate's characterization of the Cu-Ni-Si-P alloy, J. Mater. Eng. Perform. 25 (4) (2016) 1336–1341.
[27] L. Jia, H. Xie, S.P. Tao, R. Zhang, Z.L. Lu, Microstructure and selection of grain boundary phase of Cu-Ni-Si ternary alloys, Rare Metal Mater. Eng. 44 (12) (2015) 3050–3054.
[28] P.P. Freitas, L. Berger, Effect of atomic order on the electrical resistivity of alloys, Phys. Rev. B 37 (11) (1988) 6079–6084.
[29] W.D. Robertson, E.G. Grenier, V.F. Nole, The structure and associated properties of an age hardening copper alloy, Trans. Metall Soc. AIME 221 (3) (1961) 503–512.
[30] S.A. Lockyer, F.W. Noble, J. Mater. Sci. 29 (1994) 218–226.
[31] K. Toman, The structure of Ni_2Si, Acta Crystallogr. 5 (3) (1952) 329–331.
[32] S. Geller, V.M. Wolontis, The crystal structure of Co_2Si, Acta Crystallogr. 8 (2) (1955) 83–87.
[33] Y.L. Jia, M.P. Wang, C. Chen, Q.Y. Dong, S. Wang, Z. Li, Orientation and diffraction patterns of δ-Ni_2Si precipitates in Cu-Ni-Si alloy, J. Alloys Compd. 557 (25) (2013) 147–151.
[34] Y.L. Jia, Preparation and Fundamental Research of Cu-Ni-Si Alloys for Lead Frame: [D], Cent S Univ Technol (2013).
[35] X.P. Xiao, Z.Y. Yi, T.T. Chen, R.Q. Liu, H. Wang, Suppressing spinodal decomposition by adding Co into Cu-Ni-Si alloy, J. Alloys Compd. 660 (5) (2016) 178–183.
[36] Q. Lei, Z. Li, A. Zhu, W. Qiu, S. Liang, The transformation behavior of Cu-8.0Ni-1.8Si-0.6Sn-0.15Mg alloy during isothermal heat treatment, Mater. Char. 62 (9) (2011) 904–911.
[37] W. Lei, Renormalized energy for dislocations in quasi-crystals, Nonlinear Anal. 156 (6) (2017) 167–196.
[38] E. Orowan, Fracture and strength of solids, Rep. Prog. Phys. 12 (1) (1948) 185–232.
[39] M. Mabuchi, K. Higashi, Strengthening mechanisms of MgSi alloys, Acta Mater. 44 (11) (1996) 4611–4618.
[40] G. Neite, E. Nembach, Hardening mechanisms in the nimonic alloy, Mater. Sci. 29 (1985) 177–319.
[41] Q. Lei, Z. Li, M.P. Wang, L. Zhang, S. Gong, Z. Xiao, Z.Y. Pan, Phase transformations behavior in a Cu-8.0Ni-1.8Si alloy, J. Alloys Compd 8 (2011) 3617–3622.